Zentrum für Technomathematik

Fachbereich 3 – Mathematik und Informatik

Accurate Attenuation Correction in SPECT Imaging using Optimization of Bilinear Functions and Assuming an Unknown Spatially-Varying Attenuation Distribution

Ronny Ramlau **Rolf Clackdoyle**
Frédéric Noo **Girish Bal**

Report 00–14

Berichte aus der Technomathematik

Report 00–14 **September 2000**

Accurate Attenuation Correction in SPECT Imaging using Optimization of Bilinear Functions and Assuming an Unknown Spatially-Varying Attenuation Distribution

Ronny Ramlau, Rolf Clackdoyle, Frédéric Noo, and Girish Bal
Department of Radiology, University of Utah
729 Arapeen Drive, Salt Lake City, Utah 84108-1218, USA

October 14, 1999

Abstract

We report on an iterative approach to reconstruct both the activity $f(x)$ and the attenuation $\mu(x)$ directly from the emission sinogram data. The proposed algorithm is based on the iterative methods for solving linear operator equations. Whenever an operator F is the sum of a linear and a bilinear operator, a modified iteration sequence can be defined. Using a Taylor series about a fixed approximate distribution μ_0, the attenuated Radon transform can be well approximated as the sum of a linear operator in f and a bilinear operator in f and μ. The algorithm alternates between updates of f and updates of μ. In our test computations, the proposed algorithms achieve good reconstruction results both for generated and real data.

1 Introduction

Attenuation correction in SPECT imaging has been an important area of nuclear medicine research for over two decades. The measured data p can be described by the attenuated Radon transform

$$p(s,\omega) = R(f,\mu)(s,\omega) = \int_{I\!R} f(s\omega^{\perp} + t\omega) e^{-\int_t^{\infty} \mu(s\omega^{\perp}+\tau\omega)\, d\tau}\, dt \ , \tag{1}$$

($s \in \mathbb{R},\ \omega \in S^1$), which is linear in the function $f : \mathbb{R}^2 \to \mathbb{R}$ (activity function, represents the distribution of a radioactive source in an object) and nonlinear in $\mu : \mathbb{R}^2 \to \mathbb{R}$ (attenuation function, is linked to the density distribution of the object).
Since the early 1990's, the move has been toward making some measurement of the attenuation distribution using a transmission source, and incorporating the reconstructed attenuation map, $\mu(x)$, in the reconstruction of the emission distribution. More recently, there has been renewed interest in methods that achieve good attenuation correction without the use of transmission measurements. Although it is advantageous mathematically to obtain the attenuation distribution as accurately as possible, there are several practical disadvantages to making transmission

measurements. First, the additional hardware adds mechanical components to the system including long-lived radioactive sources which must be carefully and reliably shielded for patient use and increase the quality control requirements. Second, these components can increase the purchase and running costs of the scanner, especially as the transmission source usually requires periodical replacing. Third, adding transmission sources to SPECT machines can involve special requirements, such as complying with federal or state regulatory agencies for licensing, and periodical source inventory and leak-testing. Fourth, the transmission measurements may increase the total patient scanning time, unless it is performed simultaneously with the emission scan.

In a mathematical sense, the feasibility of performing accurate reconstructions with no knowledge of $\mu(x)$ has not been established. However, in many situations a complete set of transmission measurements is likely to represent "overkill" as there are cases where full knowledge of $\mu(x)$ would not be needed for attenuation correction. For example, if the emission activity $f(x)$ were essentially confined to a few specific areas (such as the heart and liver), then only a small subset of ray-sums of $\mu(x)$ would be used in a standard iterative reconstruction algorithm which incorporates attenuation information in the projection-backprojector pair. This set of ray-sums represents much less information than a full transmission scan, because from a theoretical viewpoint, these ray-sums would not be enough to perform a (hypothetical) reconstruction of $\mu(x)$.

Some efforts have been made to accurately recover the emission distribution without direct knowledge of the attenuation map. The direct approach is to consider the observed data $p(s, \omega)$ in terms of the unknown spatially-varying functions, $f(x)$ and $\mu(x)$. From here, there are two ways to proceed. First, one can try to reconstruct the attenuation map from just the emission measurements and then reconstruct the emission function by using the reconstructed attenuation map. For this purpose, a linear approximation, independent of the activity function, to the attenuated Radon transform was introduced in [4] and the inverse of this operator was used to reconstruct the attenuation map. However, the results of the reconstructions suggest that the influence of the activity function might not be negligible in many cases.

The second way, which seems to require less computational effort, is to reconstruct both the activity f and the attenuation μ simultaneously. In [5] a circular subgradient method was used to minimize the mismatch of the measured data and the computed projections with iteratively reconstructed updates for activity and attenuation. Manglos et al. [16] introduced an ART-IntraSPECT algorithm, where multiplicative updates for f and μ where computed. Both methods had only limited success due to instability problems. Another method involves Tikhonov regularization, which is a useful method to obtain stable solutions for general linear operator equations.

A new ART algorithm was recently proposed in [2]. With given measurements $p(s_l, \omega_j)$, $j = 1..N$, $l = 1..M$, the operators $R_j(f, \mu)(s) := R(f, \mu)(s, \omega_j)$ are defined. For fixed j, an update $(f + h, \mu + k)$ is computed by solving the equation $R_j(f, \mu) = R'(f, \mu)(h, k)$ in the least square sense (R'_j denotes the Frechét derivative of R_j). For different j this procedure is repeated. Numerical tests indicate a reasonable reconstruction quality, but so far no convergence or stability results are known.

Dicken [6] showed that nonlinear Tikhonov regularization can be used if one makes some rea-

sonable assumptions on the smoothness of the emission and activity functions. There the minimizing elements of the functional

$$J_\alpha(f,\mu) = \|p - R(f,\mu)\|^2 + \alpha\|(f,\mu)\|^2 \tag{2}$$

with appropriate parameter choice α are taken as approximations to the solution of (1). The difficulty in this approach is to find a convergent algorithm for the minimization of (2). Moreover, it is not clear if the minimizing functions are unique. Some iterative algorithms [9, 10, 3, 1] have been proposed for the minimization process, but the assumptions made in these papers are too strong for the case of the attenuated Radon transform.

Another general approach to the problem is to consider certain consistency conditions, published by Natterer [18] and use these as a starting point in developing algorithms. The main difference is that the consistency conditions relate the observed data to the unknown attenuation distribution μ, but do not involve the unknown emission distribution f. The idea is to get an estimate of the attenuation distribution based on the measured data, then in a second step, to incorporate this estimate into some standard reconstruction algorithm to recover the emission distribution. In all reported implementations of this approach, the attenuation map is heavily constrained. Usually the attenuation map is assumed to be constant inside some unknown boundary, and the consistency conditions are used to estimate the boundary [19, 24, 23, 17, 25]. In a recent work [13], this method has been combined with a partial transmission measurement, but the distribution for μ otherwise remains heavily constrained as usual.

In this work, the unknown attenuation distribution $\mu(x)$ is left unconstrained, and the equations linking the emission measurements to the activity distribution f and attenuation distribution μ are approximated by the sum of a linear equation in f and a bilinear equation in (f,μ). This equation is amenable to standard and stable iterative reconstruction techniques for linear problems. Some convergence and stability results for our method are given in [20]. We report on our implementation of this approach using Landweber and conjugate gradient algorithms. We have applied the algorithms to computer-simulated data and to measured phantom data. Our experimental results indicate that the method can achieve reconstruction of comparable quality to a standard approach using measured transmission data.

2 Theory

A. Algorithms

Most iteration methods for solving linear systems of the form $Tx = y$ use the *adjoint* operator T^*. In the context of tomographic reconstruction, the adjoint operator performs a backprojection operation. Mathematically, the adjoint of a linear operator T is defined by the equation $\langle Tx, y\rangle = \langle x, T^*y\rangle$, where $\langle\cdot,\cdot\rangle$ denotes the inner product in the appropriate Hilbert space. Typically an iterative algorithm can be described using a function $\mathcal{G}$ which depends on the current estimate, the adjoint operator, the pseudo-data obtained from the current estimate, and the given data:

$$x_{k+1} = \mathcal{G}(x_k, T^*, Tx_k, y). \tag{3}$$

For nonlinear systems $F(x) = y$ the adjoint is not defined, and most of the generalizations of linear methods make use of the adjoint of the Fréchet derivative F'. However, this derivative should satisfy some rather stringent theoretical conditions; it is generally assumed that an estimate of the following

$$\|F(x) - F(\tilde{x}) - F'(x)(x - \tilde{x})\| = O(\|x - \tilde{x}\|\|F(x) - F(\tilde{x})\|) \tag{4}$$

is known. For the system we are considering, $R(f, \mu) = p$, it is not known if the Fréchet derivative of $R(f, \mu)$ satisfies the required conditions.

The main idea of our method is to approximate the attenuated Radon transform by the sum of a linear operator L and a bilinear operator B:

$$R(f, \mu) \approx \tilde{R}(f, \mu) = L(f) + B(f, \mu) \ . \tag{5}$$

A bilinear operator is one which is linear in each of its arguments separately, i.e.

$$B(\alpha f_1 + \beta f_2, \mu) = \alpha B(f_1, \mu) + \beta B(f_2, \mu) \tag{6}$$
$$B(f, \alpha\mu_1 + \beta\mu_2) = \alpha B(f, \mu_1) + \beta B(f, \mu_2) \tag{7}$$

for $\alpha, \beta \in I\!R$. In order to find an approximate solution of (1) we are going to replace the operator R by its approximation and solve

$$p = \tilde{R}(f, \mu) \tag{8}$$

instead.

For fixed μ and fixed f respectively we can define linear operators

$$S_\mu(\cdot) := L(\cdot) + B(\cdot, \mu) \tag{9}$$
$$T_f(\cdot) := B(f, \cdot) \tag{10}$$

Since these operators are linear, their adjoints are defined. We now define bilinear iteration methods by extending any linear iteration method $\mathcal{G}$ to alternate between updating f and updating μ:

$$f_{k+1} = \mathcal{G}(f_k, S^*_{\mu_k}, \tilde{R}(f_k, \mu_k), p) \tag{11}$$
$$\mu_{k+1} = \mathcal{G}(\mu_k, T^*_{f_{k+1}}, \tilde{R}(f_{k+1}, \mu_k), p) \ . \tag{12}$$

In the following, we will describe the resulting methods for the *Landweber* iteration and the *conjugate gradient* method.

B. Bilinearization

The operator $\tilde{R}(f, \mu)$ is defined using a first order Taylor expansion around a known a priori guess $\mu_0(x)$ for the true attenuation map. The exponential term in equation (1) is approximated as follows:

$$e^{-\int_t^\infty (\mu_0 + \Delta\mu)(s\omega^\perp + \tau\omega)\, d\tau} \approx e^{-\int_t^\infty \mu_0(s\omega^\perp + \tau\omega)\, d\tau} \left(1 - \int_t^\infty \Delta\mu(s\omega^\perp + \tau\omega)\, d\tau\right) \ . \tag{13}$$

For $\mu_0 \neq 0$, the description given in the previous section must be modified slightly. We assume that $\mu_0(x)$ is given and fixed, and we are now interested in solving for f and $\Delta\mu$ where $\Delta\mu(x) = \mu(x) - \mu_0(x)$. Therefore we replace μ by $\Delta\mu$ in equations (5) through (12).

Combining equations (1) and (13) yields the approximation to the attenuated Radon transform,

$$\tilde{R}(f, \Delta\mu) = \int_{I\!R} f(s\omega^\perp + t\omega) e^{-\int_t^\infty \mu_0(s\omega^\perp + \tau\omega)\, d\tau} (1 - \int_t^\infty \Delta\mu(s\omega^\perp + \tau\omega) d\tau)\, dt \tag{14}$$

which is in the required form, see equation (5).

It follows that the linear operators $S_{\Delta\mu}$ and T_f are given by

$$\begin{aligned} S_{\Delta\mu}(f)(s,\omega) &= \int_{I\!R} f(s\omega^\perp + t\omega)\, e^{-\int_t^\infty \mu_0(s\omega^\perp + \tau\omega)\, d\tau} \\ &\quad \times (1 - \int_t^\infty \Delta\mu(s\omega^\perp + \tau\omega)\, d\tau)\, dt \end{aligned} \tag{15}$$

$$\begin{aligned} T_f(\Delta\mu)(s,\omega) &= -\int_{I\!R} f(s\omega^\perp + t\omega)\, e^{-\int_t^\infty \mu_0(s\omega^\perp + \tau\omega)\, d\tau} \\ &\quad \times \int_t^\infty \Delta\mu(s\omega^\perp + \tau\omega)\, d\tau\, dt\ . \end{aligned} \tag{16}$$

The corresponding adjoint operators of S_μ and T_f will be needed for the proposed iteration schemes. Using the definition of the adjoint, the following formulas can be verified. (See also [20].)

$$\begin{aligned} S^*_{\Delta\mu}(p)(x) &= \int_{S^1} p(s,\omega) e^{-\int_{x\cdot\omega}^\infty \mu_0(s\omega^\perp + \tau\omega)\, d\tau} \\ &\quad \times (1 - \int_{x\cdot\omega}^\infty \Delta\mu(s\omega^\perp + \tau\omega)\, d\tau)\, d\omega\ , \end{aligned} \tag{17}$$

$$\begin{aligned} T^*_f(p)(x) &= \int_{S^1} p(s,\omega) \int_{-\infty}^{x\cdot\omega} f(s\omega^\perp + t\omega) \\ &\quad \times e^{-\int_t^\infty \mu_0(s\omega^\perp + \tau\omega)\, d\tau}\, dt\, d\omega\ , \end{aligned} \tag{18}$$

where $s = x \cdot \omega^\perp$ everywhere inside the integrand $\int_{S^1} \ldots d\omega$.

C. Landweber–iteration

For solving a linear operator equation $Tx = y$, the Landweber iteration is defined [12, 14] by

$$x_{k+1} = x_k + \beta T^*(y - Tx_k) \ , \tag{19}$$

$0 < \beta < 1/\|T\|^2$ where $\|\cdot\|$ denotes the norm in the relevant Hilbert space. A version for nonlinear operators was described in [11]. It is well known that Landweber's method is very stable, but slow to converge. On the other hand, the performance of every iteration requires only two matrix–vector multiplications. Recent results [15, 21], using a Wavelet–compressed version of T, show that the numerical effort of Landweber iteration can be reduced reasonably. These results can easily be applied to the proposed bilinear iteration.
Using the notation of section A, the bilinear scheme takes the form

$$f_{k+1} = f_k + \beta_k S^*_{\Delta\mu_k}(p - \tilde{R}(f_k, \Delta\mu_k)) \tag{20}$$

$$\Delta\mu_{k+1} = \Delta\mu_k + \gamma_k T^*_{f_{k+1}}(p - \tilde{R}(f_{k+1}, \Delta\mu_k)) \tag{21}$$

Unlike the linear case, the scaling parameters β_k, γ_k have to be fitted to the current operators $S_{\Delta\mu_k}$ and $T_{f_{k+1}}$. Results which were obtained for bilinear operator equations [20] suggest that the parameters be chosen to satisfy $0 < \beta_k < 1/\|S_{\Delta\mu_k}\|^2$ and $0 < \gamma_k < 1/\|T_{f_{k+1}}\|^2$. In the same paper, estimates for $\|S_{\mu_k}\|$ and $\|T_{f_{k+1}}\|$ and a convergence analysis of the method can be found.

D. Conjugate Gradient method (cg)

In contrast to Landweber, the cg method is known for its rapid convergence. But, in the presence of data error, the cg method can be quite unstable. For a good review on cg and related methods we refer to [8]. Applied to our bilinearization, the cg iteration reads as follows: $f_0, \Delta\mu_0$ arbitrary, for $k = 1, \ldots$ set

$$r_k^{(1)} = S^*_{\Delta\mu_k}(p - \tilde{R}(f_k, \Delta\mu_k)) \ , \tag{22}$$

$$d_k^{(1)} = r_k^{(1)} + \beta_{k-1}^{(1)} d_{k-1}^{(1)} \ , \quad \beta_{k-1}^{(1)} = \frac{\|r_k^{(1)}\|^2}{\|r_{k-1}^{(1)}\|^2} \tag{23}$$

$$f_{k+1} = f_k + \alpha_k^{(1)} d_k^{(1)} \ , \quad \alpha_k^{(1)} = \frac{\|r_k^{(1)}\|^2}{\|\tilde{R}(f_k, \Delta\mu_k)\|^2} \ ; \tag{24}$$

$$r_k^{(2)} = T^*_{f_{k+1}}(p - \tilde{R}(f_{k+1}, \Delta\mu_k)) \ , \tag{25}$$

$$d_k^{(2)} = r_k^{(2)} + \beta_{k-1}^{(2)} d_{k-1}^{(2)} \ , \quad \beta_{k-1}^{(2)} = \frac{\|r_k^{(2)}\|^2}{\|r_{k-1}^{(2)}\|^2} \tag{26}$$

$$\Delta\mu_{k+1} = \Delta\mu_k + \alpha_k^{(2)} d_k^{(2)} \ , \ \alpha_k^{(2)} = \frac{\|r_k^{(2)}\|^2}{\|\tilde{R}(f_{k+1}, \Delta\mu_k)\|^2} \ ; \tag{27}$$

for $k = 1$ we set $d_0^{(i)} = r_0^{(i)}$, $i = 1, 2$.

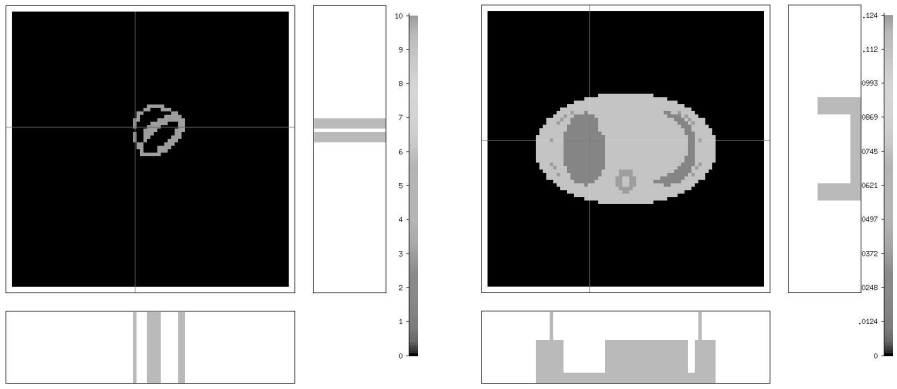

(a) (b)

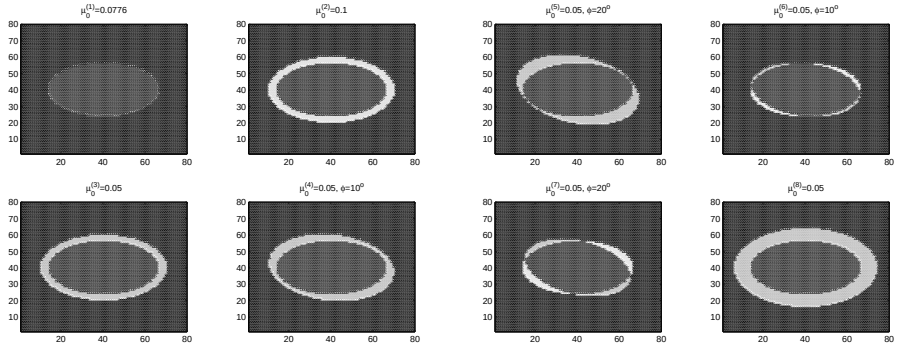

(c) (d)

Figure 1: (a): True activity distribution $f_{true}(x)$ in the heart; (b): true attenuation distribution $\mu_{true}(x)$; (c),(d): Different fixed distributions $\mu_0^{(j)}$, $j = 1...8$ used for the bilinearization of the Attenuated Radon Transform operator, $R(f, \mu)$. $\mu_0^{(1)}$ has the same support as μ_{true}; the other images show $\mu_0^{(1)} + \mu_0^{(j)}$, $j = 2, ..., 8$. The constant values used are indicated above the images.

3 Simulation studies

In this section we present some numerical results for various computer simulated data and for phantom data measured on a SPECT scanner.

A. Computer-simulated data

The standard MCAT phantom [22] was used to specify the simulated ("true") emission and transmission functions $f_{true}(x)$ and $\mu_{true}(x)$. See figure 1(a) and 1(b).

Emission data were simulated for 79 projection angles taken over 360 degrees, and a projection vector of length 80 pixels. The simulated projections included 10% additive gaussian noise. For the implementation of the bilinear Landweber and cg methods, the output $f_{rec}(x)$ and $(\mu_0 + \Delta\mu_{rec})(x)$ were discretized on an 80×80 grid. The choice of μ_0 was varied, and we report here on 8 experiments for $\mu_0^{(1)}, \mu_0^{(2)}, \ldots \mu_0^{(8)}$ all constant distributions inside an elliptical

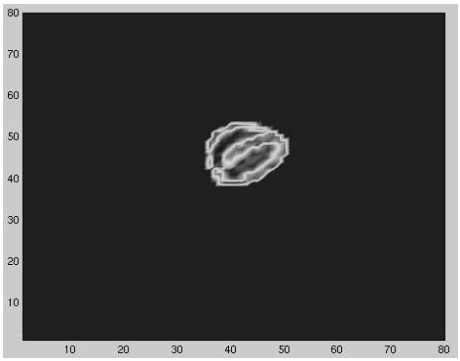

(a) Experiment 1 ($\mu_0^{(1)}$). Reconstructed emission image $f_{rec}(x)$

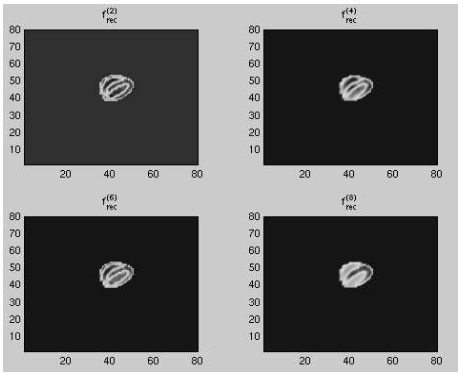

(b) Experiments 2, 4, 6, and 8. Reconstructed $f_{rec}(x)$

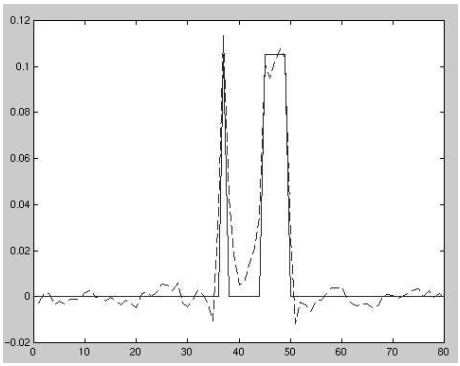

(c) Profiles of the normalized true f_{true} (solid line) and the reconstructed distribution f_{rec} (dashed line) for $y = 50$. (Experiment 1, using fixed map $\mu_0^{(1)}$)

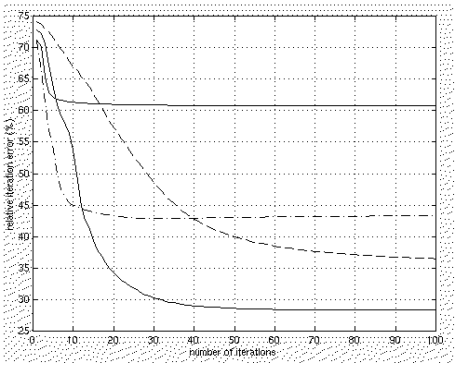

(d) Relative iteration error for different fixed maps μ_0. Lower solid line: $\mu_0^{(1)}$; dashed: $\mu_0^{(2)}$; dashdot: $\mu_0^{(6)}$; upper solid line: $\mu_0^{(8)}$.

Figure 2: Results of the reconstructions with synthetic data

region. For $\mu_0^{(1)}$ the ellipse matched the support of the true attenuation distribution and the constant value was 0.0776 cm^{-1} which was the average value in the true distribution. For the other 7 choices, the ellipse was bigger and sometimes rotated with respect to $\mu_0^{(1)}$, and the constant values were varied. See figures 1(c),1(d) for a visual description of $\mu_0^{(1)}, \mu_0^{(2)}, \ldots \mu_0^{(8)}$.

To quantitatively compare the reconstruction emission images $f_{rec}(x)$ to the true image, we first normalized both by their L^2 norm (root sum-square value). We then defined the relative error E as the L^2 norm of the difference of the normalized images, and expressed it as a percent:

$$E = \left\| \frac{f_{true}}{\|f_{true}\|} - \frac{f_{rec}}{\|f_{rec}\|} \right\| * 100\% \ .$$

Both methods were successful in reconstructing the emission function with good accuracy. The Landweber method converged much more slowly, typically requiring 20 times as many iterations to achieve the same result as the cg method. We only show the cg results here.

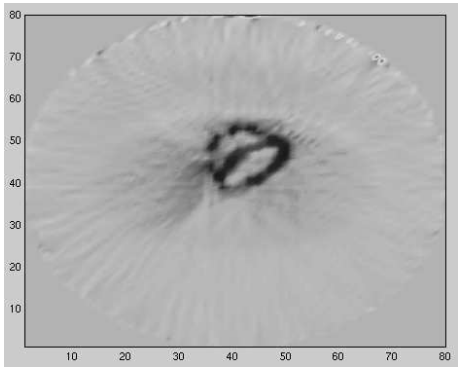

Figure 3: Reconstructed $\Delta\mu_{rec}(x)$ from experiment 1 with fixed map $\mu_0^{(1)}$

fixed map μ_0	number of iterations	relative error	max (f_{rec})
$\mu_0^{(1)}$	40	28.3%	4.2
$\mu_0^{(2)}$	100	36.5%	25
$\mu_0^{(3)}$	20	52.5%	2.5
$\mu_0^{(4)}$	20	51.6%	2.5
$\mu_0^{(5)}$	20	50.9%	2.5
$\mu_0^{(6)}$	25	42.8%	2
$\mu_0^{(7)}$	25	42.9%	2
$\mu_0^{(8)}$	30	60.8%	2.5

Table 1:Results of the reconstructions for different initial maps μ_0. For comparison, the maximum value of the true emission map was 10.

For all 8 simulations, the cg method was stopped once no improvement in relative error was detected. Table 1 shows the results obtained, including the maximum value of $f_{rec}(x)$ to give some idea of the relative normalization factors used. Figure 2(d) shows the relative error plotted as a function of iteration number for experiments 1, 2, 6, and 8. Figure 2(a) illustrates the reconstructed $f_{rec}(x)$ for experiment 1, and figure 2(b) shows $f_{rec}(x)$ for experiments 2, 4, 6, and 8. A profile through $f_{rec}(x)$ obtained from experiment 1 is shown in figure 2(c) and superimposed with the corresponding profile through $f_{true}(x)$ for comparison. The reconstructed $\Delta\mu_{rec}(x)$ is shown in figure 3.

B. Phantom Data

The Jaszczak torso phantom was filled with water and the cardiac insert was filled with approximately 4 μCi/ml of Tc-99m. The phantom was imaged on a Picker P2000 SPECT camera which simultaneously gathered emission and transmission measurements for 120 angles over 360 degrees, with a projection matrix of size 128×128. The transmission source used was Gd-153 which has a gamma emission energy of approximately 100 keV. The transmission data was scaled to account for attenuation at the Tc energy of 140 keV. One slice was extracted from each of the scan data to provide an emission sinogram $p(s, \omega)$ and an automatically registered transmission sinogram. A transmission map $\mu_{true}(x)$ was reconstructed from the transmission sinogram and incorporated into an emission reconstruction to obtain a baseline emission function $f_{true}(x)$. The emission reconstruction was performed using the linear cg method ($\mu_0(x) = \mu_{true}(x)$ and $\Delta\mu_k = 0$ for all k) and the baseline image was obtained on a grid of size 128×128. Figures 4(a) and 5(a) illustrate $\mu_{true}(x)$ and $f_{true}(x)$ respectively. For the bilinear algorithm, the function μ_0 was choosen as an ellipse containing the support of μ_{tru} and constant value inside the support.

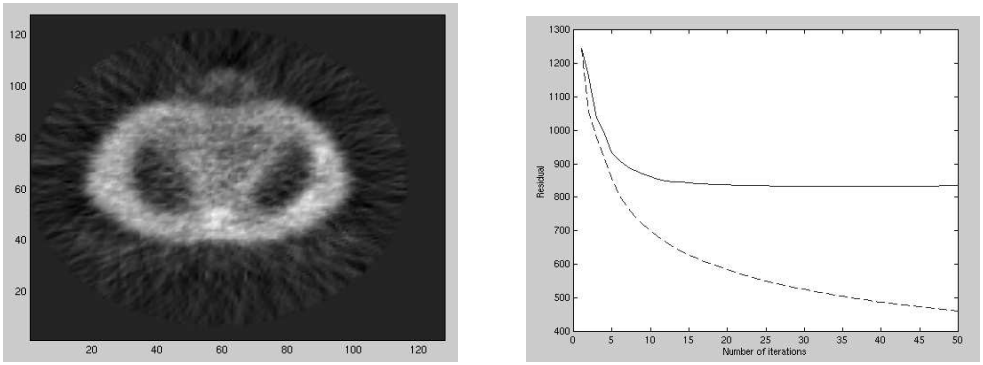

(a) (b)

Figure 4: (a):Reconstructed attenuation map $\mu_{true}(x)$. (b):Residuals versus iteration number. Solid line: reconstruction of $f_{true}(x)$ using transmission map $\mu_{true}(x)$. Dashed line: reconstruction of $f_{rec}(x)$ using bilinear cg method.

4 Discussion and Conclusions

From the results of the computer simulation experiments, we observe that absolute quantitative reconstructions do not seem possible using our approach. The values in the last column of the table indicated that the magnitude of the image can vary greatly with different starting conditions μ_0 although the visual quality of the images are relatively similar. (Compare figures 2(a) and 2(b) to figure 1(a).) The cause of these magnitude variations is linked to the choice of μ_0. For instance, taking a larger value for the constant inside the ellipse or taking a larger ellipse both mean a smaller exponential term and therefore one expects the values for f to be

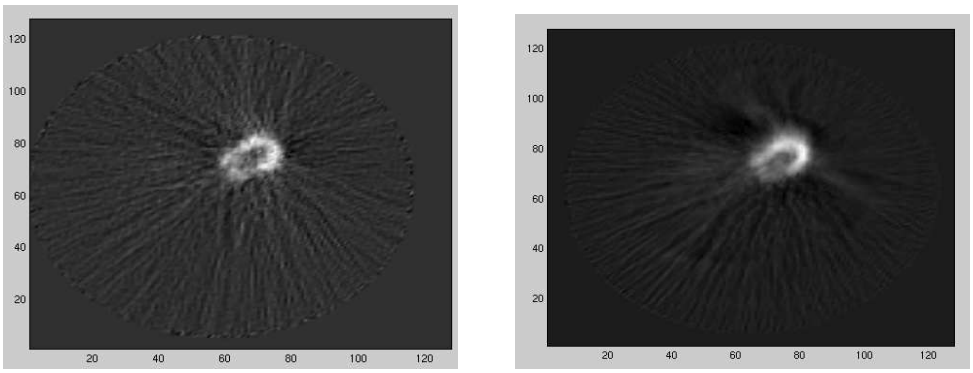

(a) Reconstructed emission map $f_{true}(x)$, using $\mu_{true}(x)$.

(b) Reconstructed emission map, bilinear cg. No measured transmission data was used.

Figure 5: Results of the reconstructions with real data

bigger. This pattern is apparent in table 1. For given data y, the operator equation $R(f, \mu) = y$ (as a function of μ) has no unique solution. Thus we expect our algorithm to converge to a solution in a neighborhood of μ_0.

The accuracy of the normalized images also depended strongly on the choice of μ_0. The relative errors listed in table 1 show that there was a direct connection between the quality of the reconstruction and the chosen μ_0. As one might expect, a good estimate for μ_0 gave a good reconstruction, whereas $\mu_0^{(8)}$, which is the worst estimate, yielded the worst result. Assuming a certain smoothness of the solution of a linear equation $Tx = y$, it is a well known result [14, 7] that, for given data y^δ with noise level δ, the reconstruction error can be bounded by $\delta^{1/2}$: $\|x - x_{rec}\| = O(\delta^{1/2})$. In our example, this would yield a best possible (relative) upper error bound of approximately 40%. Thus, the maps 2, 6, and 7 still produced good results, and map 1 with a correct estimate for the support of the attenuation map and with a good average value of μ gave the best reconstruction.

It is apparent from these observation, that the choice of μ_0 dominates where the reconstruction will converge, with $\Delta\mu$ only making small adjustments. A probable reason for this behavior would be a large number of local minimum, all lying close to virtually any specified μ_0. The reconstruction of $\mu(x)$ must therefore be generally very poor, and indeed, figure 3 illustrates the classical behavior of a "negative" emission image superimposed on the solution to the attenuation distribution.

Visual inspection of the phantom experiment images indicates that similar quality reconstructions were achieved although our bilinear method produced a smoother image than the standard approach using measured transmission data. However, the plot of the residuals, figure 4(b), seemed to suggest that the bilinear method was better able to match the measured data. It may be that a more sensitive test is needed to establish whether improved reconstruction quality is occurring. One possible explanation for the poorer data match when using transmission scan is that the measurements obtained will not be ideal in terms of the Tc emission scan. The bilinear method is able to adjust the $\mu(x)$ map to improve the data match, whereas the

linear cg method had a rigid and perhaps slightly inaccurate attenuation map to work from.

We observed some of the expected features of the conventional Landweber and cg methods. To obtain the same reconstruction quality, the cg method only needed about 20 iterations compared to 400 iterations of the bilinear Landweber method. This factor dominates the effect of the more complicated and slower update for the cg method. In our current implementation, a full cg iteration (one update for f and μ) needed 70 seconds of cpu time compared to 48 seconds for Landweber. Both algorithms demonstrated high stability. Stability was expected for the bilinear Landweber method, but we were quite surprised to observe the same result for cg. Usually, in the presence of data error, cg will quickly approach the sought solution but after arriving at some minimal distance, it will diverge. This did not happen in our experiments.

Our bilinear method relies on a good bilinear estimate $\tilde{R}(f, \Delta\mu)$ to the attenuated Radon transform $R(f, \mu)$. Clearly, the estimate depends on how closely μ_0 approximates the true μ distribution. For a practical example, note that $e^{-\Delta}$ is approximated by $1 - \Delta$ to within 5% if $|\Delta| < 0.28$. Therefore, the operator R is approximated uniformly to within 5% by $\tilde{R}$ if

$$|\int_t^\infty \mu(s\omega^\perp + \tau\omega)\, d\tau - \int_t^\infty \mu_0(s\omega^\perp + \tau\omega)\, d\tau| < 0.28 \tag{28}$$

for all ω, s, and t. Considering an attenuation length of 40 cm for the torso of a large patient, the a priori distribution μ_0 should not deviate by more than 0.007 cm^{-1} from the true attenuation on average. Note that (28) is only of interest if $s\omega + t\omega^\perp \in supp\ f$. Often $supp\ f$ can be much smaller than $supp\ \mu$. As a consequence, the real attenuation length on each line will be less than 40 cm and (28) provides only a coarse worst-case estimate. If an μ_0 is taken to be some constant average value within a reasonably well estimated boundary, then a 5% uniform bound should be achievable.

One possibility to enhance this method would be to make use of higher terms of the Taylor series for the exponential function. The attenuated Radon transform is then replaced by a multilinear operator, $R(f, \mu_0 + \Delta\mu) \approx A(f) + B(f, \Delta\mu) + C(f, \Delta\mu, \Delta\mu) + D(f, \Delta\mu, \Delta\mu, \Delta\mu) \cdots$ Similar to (5)-(11), an n-step iteration scheme can be defined. The new approximation to R would be better than the bilinearization used in our paper. Thus, we might expect better reconstruction results, especially with a bad guess for μ_0.

In conclusion, we have found that the cg bilinear method is effective in producing an attenuation corrected reconstruction without transmission measurements, but the technique relies on a good choice of the fixed attenuation map $\mu_0(x)$. A good fixed attenuation map is needed both to maintain the integrity of the Taylor approximation used to define the bilinear operator $\tilde{R}(f, \Delta\mu)$, and to provide good emission reconstructions (low relative error). Quantitative accuracy of the reconstructions depends very heavily on how well μ_0 approximates the true attenuation distribution.

Our bilinear method might also have useful applications even when the transmission measurements are made. By setting μ_0 equal to the reconstructed transmission map, our method will automatically fine-tune the attenuation distribution as it searches for the accurate emission distribution.

5 Acknowledgements

This work was partially support by the DAAD, and partially supported by NIH grant R29 HL55610-03. F Noo is *Chargé de Recherche* with the FNRS, Belgium.

References

[1] A. W. Bakushinskii. The problem of the convergence of the iteratively regularized gauss–newton method. *Comput. Maths. Math. Phys.*, (32):1353–1359, 1992.

[2] S. Biedenstein. *Adaptive Schwächungskorrektur in der Einzelphotonen-Emissions-Computer-Tomographie mittels Simultaner Iterativer Rekonstruktion von Emission und Absorption.* Ph.d. thesis, Universität Münster, 1998.

[3] B. Blaschke, A. Neubauer, and O. Scherzer. On convergence rates for the iteratively regularized gauss–newton method. *IMA Journal of Numerical Analysis*, (17):421–436, 1997.

[4] A. V. Bronnikov. Approximate reconstruction of attenuation map in SPECT imaging. *IEEE Trans. Nucl. Sci.*, (42):1483–1488, 1995.

[5] Y. Censor, D. Gustafson, A. Lent, and H. Tuy. A new approach to the emission computerized tomography problem: simultaneous calculation of attenuation and activity coefficients. *IEEE Trans. Nucl. Sci.*, (26):2275–79, 1979.

[6] V. Dicken. *Simultaneous Activity and Attenuation Reconstruction in Single Photon Emission Computed Tomography, a Nonlinear Ill-Posed Problem.* Ph.d. thesis, Universität Potsdam, 5/ 1998.

[7] H. W. Engl, M. Hanke, and A. Neubauer. *Regularization of Inverse Problems.* Kluwer, Dordrecht, 1996.

[8] M. Hanke. *Conjugate gradient type methods on ill-posed problems.* Longman, 1995.

[9] M. Hanke. A regularizing levenberg–marquardt scheme, with applications to inverse groundwater filtration problems. *Inverse Problems*, (13):79–95, 1997.

[10] M. Hanke. Regularizing properties of a truncated newton–cg algorithm for nonlinear ill-posed problems. *Numer. Funct. Anal. Optim.*, (18):971–993, 1997.

[11] M. Hanke, A. Neubauer, and O. Scherzer. A convergence analysis of the Landweber iteration for nonlinear ill-posed problems. *Numerische Mathematik*, (72):21–37, 1995.

[12] L. Landweber. An iteration formula for fredholm integral equations of the first kind. *Amer. J. Math.*, (73):615–624, 1951.

[13] I. Laurette, R. Clackdoyle, A. Welch, F. Natterer, and G. T. Gullberg. Comparison of three applications of ConTraSPECT. *IEEE Trans. Nucl. Sci. (Accepted for publication)*, 1999.

[14] A. K. Louis. *Inverse und schlecht gestellte Probleme.* Teubner, Stuttgart, 1989.

[15] P. Maass and R. Ramlau. Wavelet-accelerated regularization methods for hyperthermia treatment planning. *Int. Journal of Imaging Systems and Technology*, (7):191–199, 1996.

[16] S. H. Manglos and T. M. Young. Constrained intraSPECT reconstructions from SPECT projections. In *Conf. Rec. IEEE Nuclear Science Symp. and Medical Imaging Conference, San Francisco, CA*, pages 1605–1609. 1993.

[17] S. C. Moore, S. P. Kijewski, and S. P. Mueller. A general approach to nonuniform attenuation correction using emission data alone. *Journal of Nuclear Medicine*, (38):68P, 1997.

[18] F. Natterer. Computerized tomography with unknown sources. *SIAM J. Appl. Math.*, (43):1201–12, 1983.

[19] F. Natterer. Determination of tissue attenuation in emission tomography of optically dense media. *Inverse Problems*, (9):731–736, 1993.

[20] R. Ramlau. Iterative solutions of bilinear ill posed problems. Submitted for publication.

[21] R. Ramlau. A modified landweber–method for inverse problems. *Numerical Functional Analysis and Optimization*, 20(1& 2), 1999.

[22] J. A. Terry, B. M. W. Tsui, J. R. Perry, J. L. Hendricks, and G T Gullberg. The design of a mathematical phantom of the upper human torso for use in 3-d SPECT imaging research. In *Proc. 1990 Fall Meeting Biomed. Eng. Soc. (Blacksburg, VA)*, pages 1467–74. New York University Press, 1990.

[23] A. Welch, R. Clack, P. E. Christian, and G. T. Gullberg. Toward accurate attenuation correction without transmission measurements. *Journal of Nuclear Medicine*, (37):18P, 1996.

[24] A. Welch, R. Clack, G. T. Gullberg, and F. Natterer. Accurate attenuation correction in SPECT without transmission measurements. In *Conf. Rec. IEEE Nuclear Science Symp. and Medical Imaging Conference, San Francisco, CA*, pages 939–943. 1995.

[25] A Welch, R Clack, F Natterer, and G T Gullberg. Toward accurate attenuation correction in SPECT without transmission measurements. *IEEE Trans. Med. Imaging*, (16):532–40, 1997.

Berichte aus der Technomathematik ISSN 1435-7968

http://www.math.uni-bremen.de/zetem/berichte.html

— Vertrieb durch den Autor —

Reports **Stand: 13. September 2000**

98–01. Peter Benner, Heike Faßbender:
An Implicitly Restarted Symplectic Lanczos Method for the Symplectic Eigenvalue Problem, Juli 1998.

98–02. Heike Faßbender:
Sliding Window Schemes for Discrete Least-Squares Approximation by Trigonometric Polynomials, Juli 1998.

98–03. Peter Benner, Maribel Castillo, Enrique S. Quintana-Ortí:
Parallel Partial Stabilizing Algorithms for Large Linear Control Systems, Juli 1998.

98–04. Peter Benner:
Computational Methods for Linear–Quadratic Optimization, August 1998.

98–05. Peter Benner, Ralph Byers, Enrique S. Quintana-Ortí, Gregorio Quintana-Ortí:
Solving Algebraic Riccati Equations on Parallel Computers Using Newton's Method with Exact Line Search, August 1998.

98–06. Lars Grüne, Fabian Wirth:
On the rate of convergence of infinite horizon discounted optimal value functions, November 1998.

98–07. Peter Benner, Volker Mehrmann, Hongguo Xu:
A Note on the Numerical Solution of Complex Hamiltonian and Skew-Hamiltonian Eigenvalue Problems, November 1998.

98–08. Eberhard Bänsch, Burkhard Höhn:
Numerical simulation of a silicon floating zone with a free capillary surface, Dezember 1998.

99–01. Heike Faßbender:
The Parameterized SR Algorithm for Symplectic (Butterfly) Matrices, Februar 1999.

99–02. Heike Faßbender:
Error Analysis of the symplectic Lanczos Method for the symplectic Eigenvalue Problem, März 1999.

99–03. Eberhard Bänsch, Alfred Schmidt:
Simulation of dendritic crystal growth with thermal convection, März 1999.

99–04. Eberhard Bänsch:
Finite element discretization of the Navier-Stokes equations with a free capillary surface, März 1999.

99–05. Peter Benner:
Mathematik in der Berufspraxis, Juli 1999.

99–06. Andrew D.B. Paice, Fabian R. Wirth:
Robustness of nonlinear systems and their domains of attraction, August 1999.

99–07. Peter Benner, Enrique S. Quintana-Ortí, Gregorio Quintana-Ortí:
Balanced Truncation Model Reduction of Large-Scale Dense Systems on Parallel Computers, September 1999.

99–08. Ronald Stöver:
Collocation methods for solving linear differential-algebraic boundary value problems, September 1999.

99–09. Huseyin Akcay:
Modelling with Orthonormal Basis Functions, September 1999.

99–10. Heike Faßbender, D. Steven Mackey, Niloufer Mackey:
Hamilton and Jacobi come full circle: Jacobi algorithms for structured Hamiltonian eigenproblems, Oktober 1999.

99–11. Peter Benner, Vincente Hernández, Antonio Pastor:
On the Kleinman Iteration for Nonstabilizable System, Oktober 1999.

99–12. Peter Benner, Heike Faßbender:
A Hybrid Method for the Numerical Solution of Discrete-Time Algebraic Riccati Equations, November 1999.

99–13. Peter Benner, Enrique S. Quintana-Ortí, Gregorio Quintana-Ortí:
Numerical Solution of Schur Stable Linear Matrix Equations on Multicomputers, November 1999.

99–14. Eberhard Bänsch, Karol Mikula:
Adaptivity in 3D Image Processing, Dezember 1999.

00–01. Peter Benner, Volker Mehrmann, Hongguo Xu:
Perturbation Analysis for the Eigenvalue Problem of a Formal Product of Matrices, Januar 2000.

00–02. Ziping Huang:
Finite Element Method for Mixed Problems with Penalty, Januar 2000.

00–03. Gianfrancesco Martinico:
Recursive mesh refinement in 3D, Februar 2000.

00–04. Eberhard Bänsch, Christoph Egbers, Oliver Meincke, Nicoleta Scurtu:
Taylor-Couette System with Asymmetric Boundary Conditions, Februar 2000.

00–05. Peter Benner:
Symplectic Balancing of Hamiltonian Matrices, Februar 2000.

00–06. Fabio Camilli, Lars Grüne, Fabian Wirth:
A regularization of Zubov's equation for robust domains of attraction, März 2000.

00–07. Michael Wolff, Eberhard Bänsch, Michael Böhm, Dominic Davis:
Modellierung der Abkühlung von Stahlbrammen, März 2000.

00–08. Stephan Dahlke, Peter Maaß, Gerd Teschke:
Interpolating Scaling Functions with Duals, April 2000.

00–09. Jochen Behrens, Fabian Wirth:
A globalization procedure for locally stabilizing controllers, Mai 2000.

00–10. Peter Maaß, Gerd Teschke, Werner Willmann, Günter Wollmann:
Detection and Classification of Material Attributes – A Practical Application of Wavelet Analysis, Mai 2000.

00–11. Stefan Boschert, Alfred Schmidt, Kunibert G. Siebert, Eberhard Bänsch, Klaus-Werner Benz, Gerhard Dziuk, Thomas Kaiser:
Simulation of Industrial Crystal Growth by the Vertical Bridgman Method, Mai 2000.

00–12. Volker Lehmann, Gerd Teschke:
Wavelet Based Methods for Improved Wind Profiler Signal Processing, Mai 2000.

00–13. Stephan Dahlke, Peter Maass:
A Note on Interpolating Scaling Functions, August 2000.

00–14. Ronny Ramlau, Rolf Clackdoyle, Frédéric Noo, Girish Bal:
Accurate Attenuation Correction in SPECT Imaging using Optimization of Bilinear Functions and Assuming an Unknown Spatially-Varying Attenuation Distribution, September 2000.